Micro-photoluminescence of carbon dots deposited on twisted double-layer graphene grown by chemical vapor deposition

Journal:	*ACS Applied Materials & Interfaces*
Manuscript ID	am-2020-21853d.R1
Manuscript Type:	Article
Date Submitted by the Author:	n/a
Complete List of Authors:	FAGGIO, Giuliana; Universita degli Studi Mediterranea di Reggio Calabria, DIIES Grillo, Rossella; Università degli Studi Mediterranea di Reggio Calabria Facoltà di Ingegneria, DIIES Foti, Antonino; Consiglio Nazionale delle Ricerche, IPCF Agnello, Simonpietro; Universita degli Studi di Palermo, of Physics and Chemistry Messina, Fabrizio; Universita degli Studi di Palermo, Dipartimento di Fisica e Chimica Messina, Giacomo; Università "Mediterranea", 2Dipartimento di Meccanica e Materiali, Facoltà di Ingegneria

Micro-photoluminescence of carbon dots deposited on twisted double-layer graphene grown by chemical vapor deposition

Giuliana Faggio[†,*], *Rossella Grillo*[†], *Antonino Foti*[†,#], *Simonpietro Agnello*[§], *Fabrizio Messina*[§], *Giacomo Messina*[†]

[†]Department of Information Engineering, Infrastructures and Sustainable Energy (DIIES), University "Mediterranea" of Reggio Calabria,Loc. Feo di Vito, 89122 Reggio Calabria, Italy

[#]Present address: IPCF-CNR, Institute for Chemical and Physical Processes, National Research Council, Viale F. Stagno D'Alcontres 37, I-98158 Messina, Italy

[§]Department of Physics and Chemistry Emilio Segre', University of Palermo, Via Archirafi 36, 90143 Palermo, Italy

KEYWORDS: carbon dots, twisted bilayer graphene, Raman spectroscopy, micro-photoluminescence, AFM

ABSTRACT. Carbon-based nanomaterials, such as carbon dots (CDs) and graphene (Gr), feature outstanding optical and electronic properties. Hence their integration in optoelectronic and photonic devices, easier thanks to their low dimensionality, offers the possibility to reach high-quality performances. In this context the combination of CDs and Gr into new nanocomposite materials CDs/Gr can further improve their optoelectronic properties and eventually create new ones, paving the way for the development of advanced carbon nanotechnology. In this work we have thoroughly investigated the structural and emission properties of CDs deposited on single and bilayer graphene lying on a SiO_2/Si substrate. A systematic Raman analysis points out that bilayer (BL) graphene grown by chemical vapour deposition does not always respect the Bernal (AB) stacking but it is rather a mixture of twisted bilayer (t-BL) featuring domains with different twist angles. Moreover in-depth micro-photoluminescence measurements, combined with atomic force microscopy (AFM) morphological analysis, show that CDs emission efficiency is strongly depleted by the presence of graphene and in particular is dependent on the number of layers as well as on the twist angle of BL graphene. Finally we propose a model which explains these results on the basis of photoinduced charge transfer processes taking into account the energy levels of the hybrid nano-system formed by coupling CDs with t-BL/SiO_2.

1. INTRODUCTION

Nanotechnologies are expanding into several fields of applied science. The growing industrial demand pushes the scientific community to design new nanomaterials with properties tailored for specific applications. The combination of nanomaterials with exceptional physical properties paves the way for the development of new generation of materials whose benefits exceed those of the individual components.

Nanocomposite materials based on carbon dots (CDs) and graphene are proving to be very promising materials in many applications such as photovoltaics and photo-catalysis.[1,2] The unique combination of the optical properties of CDs with the electronic properties of graphene offers new opportunities for fabricating all-carbon optoelectronic and photonic devices.[3] CDs are luminescent carbon nanoparticles that, since their discovery in 2004, have attracted the attention of the scientific community due to their versatile optical properties.[4] CDs have generally diameter smaller than 10 nm and consist of an amorphous and/or crystalline carbon core surrounded by superficial functional groups. Both the core and the superficial groups have a significant influence on the CD's emission mechanism.[5] CDs show large charge transfer efficiency, bright and tunable fluorescence, and photo-stability. They can be easily synthesized in water-based solvents and present low toxicity and biocompatibility. For all these reasons, together with the natural abundance of carbon precursors, CDs gained popularity in many fields such as photo-catalysis, [1,6] optoelectronics,[3,7,8] and energy harvesting.[9,10] A recent study[11] used nitrogen-doped graphene quantum dots deposited on the top of an inorganic γ-$CsPbI_3$ perovskite solar cell to harvest and convert UV light into visible light for improved solar cell efficiency beyond 16%.

Graphene, a two-dimensional layer of carbon atoms with sp^2 hybridization arranged in a honeycomb lattice, is characterized by excellent electronic, optical and mechanical properties, which are mainly due by its atomic thickness and structure.[12–15] Single layer (SL) graphene can be

produced either by mechanical exfoliation of graphite or by various synthesis methods including epitaxial growth and chemical vapor deposition (CVD) on selected substrates.[12,16–19] Beside the SL, CVD technique allows also the production of bilayer (BL) or few layers graphene,[20] which still present unique electronic, optical and mechanical properties.[21–23] It has been reported that part of the BL graphene obtained via CVD is twisted,[24–28] meaning that the two graphene layers forming the BL are rotated by a relative twist angle (θ), which translates in a stacking order that differs from the well-known AB (or Bernal) and AA stackings (in which the atoms of the upper layer are perfectly aligned to the atoms of the bottom layer).[21,29,30]

Considerable efforts have been devoted over the last decade to investigate the dependence of the physical properties in BL graphene on the twist angle.[21,22,24,26,27,31–34] It has been proven that the electronic and optical properties of twisted bilayer (t-BL) graphene are quite different from that of AB-BL as well as that of SL.[35,36] This allows to expand their potentialities and application fields.[37] In t-BL the behavior of charge carriers changes with rotational angle. In particular, the electronic interlayer coupling decreases with the increase of the twist angle.[38] At large twist angle the electronic properties become more similar to those of a single layer of graphene. [39] The tunability of t-BL electronic, optical and thermal properties, arising from the twist angle dependence, makes them excellent candidates for applications in optoelectronic devices, such as transparent electrodes for solar cells and photonic crystals.[40,41]

CDs/graphene composites are commonly synthetized in liquid phase using graphene oxide, mainly for photo-catalysis applications.[1] However, if one wants to extend their field of application to optoelectronic devices, it is necessary to study CDs/graphene composites in the solid phase and to evaluate their interaction with target substrates. Recently, N-doped carbon quantum dots/graphene material was used as photoactive electrode for UV sensing in an electrochemical cell.[42]Chen et

al.[43] demonstrated that adding carbon quantum dots to graphene improved the photoresponsivity of graphene/silicon Schottky-junction photodetector. Moreover, films composed of quantum dots of different materials ($CsPbI_3$) and micrometer-sized graphene sheets were successfully used to improve the efficiency and stability of all-inorganic perovskite solar cells.[44]

The interaction between CDs and SL graphene in solid phase modifies the CDs emission mechanism leaving the structure of the graphene unchanged.[17] The quenching of CDs photoluminescence (PL) observed in the CDs/SL graphene composites was explained with a charge transfer between CDs and SL graphene.[45]

In this work, we report a systematic study on the structural and emission properties of CDs on t-BL graphene grown by CVD, supported on SiO_2 substrate. The surface morphology and the structural properties of the system were investigated by optical, scanning electron microscopy (SEM) and Atomic Force Microscopy (AFM) as well as micro-Raman spectroscopy, respectively. The emission efficiency of CDs deposited on the t-BL/SiO_2/Si substrates was investigated by micro-photoluminescence (μPL) measurements exciting with 2.62 eV (473 nm) laser energy. In particular, the CDs emission efficiency is observed to be strongly dependent on the twist angle and thus on the interlayer coupling. Finally, we propose a model to explain the charge transfer process from CDs to t-BL/SiO_2/Si substrate. Our model is based on the competition between two electron transfer mechanisms, a radiative and a non-radiative one, whose prevalence of one over the other is linked to the interlayer coupling degree and then to Fermi velocity renormalization.

2. EXPERIMENTAL SECTION

Large area, polycrystalline graphene films with bilayer islands were purchased from Graphene Laboratories Inc. Such films were first grown by CVD on copper foils and then transferred on p-doped silicon wafers with 90 nm silicon dioxide coating via the PMMA assisted transfer method.[19,46,47]

CDs were synthesized by thermally induced decomposition of organic precursors, as previously reported.[48] In brief, aqueous solutions of citric acid monohydrate and urea (3 g in 10 mL Milli-q water) were mixed and used as carbon and nitrogen precursors, respectively. The mixture was then exposed to microwave irradiation till the water completely evaporated. This method results in CDs with an average size of 5 nm, having crystalline core structure and surface-functionalization with amide and carboxylic groups.[49] The as-synthesized CD powder was then dispersed in ethanol at a final concentration of 0.1 g/L.

For the preparation of CDs/Gr sample, CDs dispersion was diluted by a factor 104 in volume of the stock solutions. Subsequently, 1 μL of the diluted dispersion was deposited onto the $Gr/SiO_2/Si$ sample via drop-casting technique.

Micro-Raman and micro-PL spectroscopy measurements were carried out at room temperature with a HORIBA Scientific LabRAM HR Evolution Raman spectrometer with an integrated Olympus BX41 microscope. A laser excitation wavelength of 473 nm (2.62 eV) was focused on the sample surface using a 100× objective with a spot size of approximately 0.7 μm in diameter. Low laser power (below 1 mW) was used to minimize sample heating and possible damages. In addition, a co-localized AFM/Raman setup allows to obtain the simultaneous acquisition of overlapped AFM and Raman maps.

Amplitude modulation AFM (AM-AFM) measurements were performed in air using an AIST-NT SmartSPM operating in tapping mode. The system is equipped with a conventional piezoscanner (maximum xy range 100 μm and maximum z range 15 μm) and a four-segment photodetector for cantilever deflection monitoring. The AFM is integrated with a camera and an optical microscope so that a precise tip positioning is achievable. We used AppNano Silicon-SPM-probes designed to allow a direct optical view of the AFM tip when imaging for co-localized Raman and AFM measurements, with Al backside reflex coating having a resonance frequency ~300 kHz and a tip apical diameter of 6 nm. All the scans were performed at room temperature. The scan rate was set to 1 Hz in order to minimize the artefacts due to the thermal drift[50]. The oscillation amplitude was set in the range between 20 to 100 nm, depending on the expected surface topography. Measurements were made in a minimum of three different areas of each sample in order to account for homogeneities which might derive from the sample preparation. Within each area, a minimum of five well-separated 15 × 15 μm sites were scanned and the scan size gradually decreased.

3. RESULTS AND DISCUSSION

3.1 Spectroscopic Characterization

The commercial single/double CVD graphene used in this work was preliminarily characterized by co-localized AFM/Raman analysis. Such analysis involves the simultaneous acquisition of AFM images and Raman maps, in order to obtain information on the morphology and structure of the same sample area.

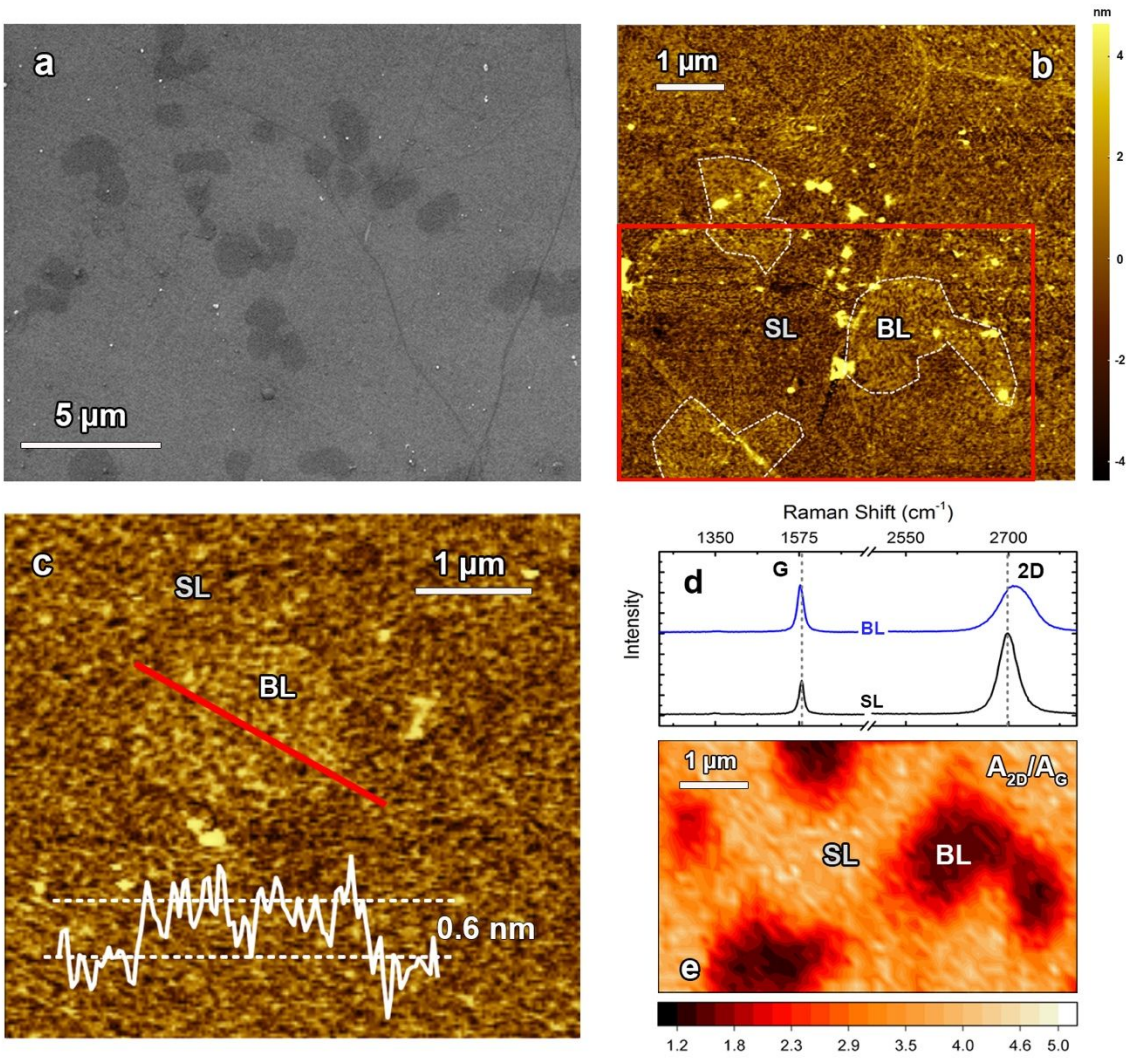

Figure 1. (a) SEM image of the as bought graphene film on SiO_2/Si with no CDs deposited over the surface. The darker spots correspond to the bilayer areas. Wrinkles (dark lines) and impurities (bright spots) are also visible. (b) A 7 µm x 7 µm AFM image that confirms the presence of several bilayer domains (white dash contoured) as well as of impurities and wrinkles. (c) 5 µm x 5 µm representative AFM image displaying a bilayer island. The top layer shows a brighter color with respect to the monolayer graphene in the background. The profile measured along the red line shows the height of the top layer. (e) Raman imaging of A_{2D}/A_G ratio of the area marked by the red rectangle in (b), with two representative Raman spectra of the BL (blue line) and SL (black line) graphene shown in panel (d). The Raman images were obtained by collecting more than 1900 spectra over an area of about 6 µm x 4 µm, with a step size of 100 nm.

Figure 1a shows a representative image of the graphene on SiO_2/Si substrate taken with a scanning electron microscope (SEM). The different contrast clearly highlights the presence of BL graphene

areas[51] (darker spots) and wrinkles (probably due to the transfer process) on top of a nearly homogeneous SL graphene. An optical image of the sample is also given in Figure S1. Further AFM investigation was performed in order to better study the morphology of the sample. **Figure 1b** shows a typical AFM image of the sample. Several BLs graphene, recognizable by a slightly lighter color with respect to the background and highlighted by a white dashed line, are present together with wrinkles ad some impurities (the bright spots in the image). These impurities are most likely PMMA contaminations caused by the transfer procedure. The BL graphene areas have irregular shape and dimensions within the range of 1-2 μm. The line profile measured across a typical BL graphene (red line in Figure 1c) reveals a thickness of the top layer of approximately 0.6 nm. This value is in agreement with other AFM studies of single and few layers graphene, where the thickness of a single graphene sheet is observed up to 1 nm.[32,52–54] The difference with the expected theoretical value of 0.34 nm relatively to single layer thickness[55] is attributable to many factors, including variations in the tip–sample interaction and different free oscillation amplitude values of the tapping cantilever[53] as well as a different stacking order in t-BL graphene.[32] The crystalline quality of the as-bought single/double graphene film was assessed by Raman spectroscopy. As mentioned above, co-localized AFM/Raman technique provides the advantage of acquiring overlapped Raman and AFM images with pixel-to-pixel correspondence. Representative Raman spectra relative to SL and BL graphene are shown in **Figure 1d**. The Raman spectrum of SL graphene (black curve) reveals the *G* band at ~ 1580 cm^{-1} and the *2D* band at ~ 2699 cm^{-1}. A blue shift of ~11 cm^{-1} is observed for the *2D* band position of BL graphene (blue curve) with respect to SL one.[56] The absence of the *D* band at ~1350cm^{-1}, which indicates the presence of structural defects, confirms the high quality of the sample.[57,58] It should be underlined the absence of any photoluminescence in the above reported SL and BL graphene spectra.

Figure 1e displays the Raman imaging of *2D* to *G* peak integrated intensity ratio (A_{2D}/A_G) of the area marked by the red rectangle in **Figure1b**. The Raman map shows $A_{2D}/A_G > 4.0$, typical signature of SL graphene, and lower values ($A_{2D}/A_G \cong 1.5$) in dark areas confirming BL graphene formation.[25]

The single/double graphene sample was covered with CDs by drop-casting technique and carefully characterized to evaluate the morphology, as well as the structural and emission properties. We chose a region near the center of the drop, in order to avoid big CDs clusters due to the coffee-ring effect. **Figure 2** shows simultaneously acquired topography image (**Figure 2a**), μPL map (**Figure 2b)** and *2D* peak integrated intensity (A_{2D}) Raman map (**Figure 2c**) of the deposited sample. The CDs are distributed on the whole surface, including both the graphene (from now on referred as CDs/SL) and the SiO_2 (henceforward indicated as CDs/SiO_2). The CDs spread on both substrates is uniform as highlighted by green height profile traced along the dashed line in **Figure 2a** and by comparing the image with the morphology of the substrate with no CDs (**Figure S2**). The increase of the surface roughness is, in fact, compatible with the typical CDs size. Representative Raman/μPL spectra of CDs/SL and CDs/SiO_2 are compared to that of the bare SL graphene (**Figure2d)**. Si Raman peaks (305 cm^{-1}, 520 cm^{-1} and 960 cm^{-1})[59] are common to all spectra. A large PL band centered at about 2.36 eV characterizes CDs/SiO_2 spectrum (red curve), while the CDs/SL spectrum (blue curve) exhibits the characteristic *G* and *2D* graphene Raman bands superimposed to a background CDs PL band centered at ~2.32 eV.[48,49] It is worth to note that the sample of graphene features a low intensity *D* band both in the naked and in the CDs covered region, underlying that the quality of the graphene is not modified by the deposition. The strong PL contribution dominates the interaction between CDs and light on the SiO_2 surface.[60] On the other side, it is not surprising to find that the intensity of the PL band is significantly quenched

when the CDs are deposited on graphene. This is in line with previous studies, where the quenching effect of CDs PL due to graphene was observed by exciting the CDs/SL samples with a laser wavelength of 532 nm (2.33 eV). [17,45,60]

In order to emphasize this effect, a line profile measured along the dashed lines in **Figure2a-c** is reported in **Figure2e-g**. Here, in correspondence of the area covered by graphene, CDs PL undergoes a strong intensity reduction if compared to the μPL level observed on the region uncovered by graphene, i.e. the SiO_2 substrate (**Figure 2f**), as also confirmed by the line profile of A_{2D} (**Figure 2g**), increasing as the PL is dropping, and the topography height profile acquired with AFM (**Figure 2e**), which allowed us to measure a SL graphene thickness of 1 nm when lying on SiO_2/Si.

The presence of many double layers in the commercial CVD graphene analysed, induced us to carry out a more detailed μPL spectroscopy investigation on the emission properties of CDs interacting with BL graphene (CDs/BL).

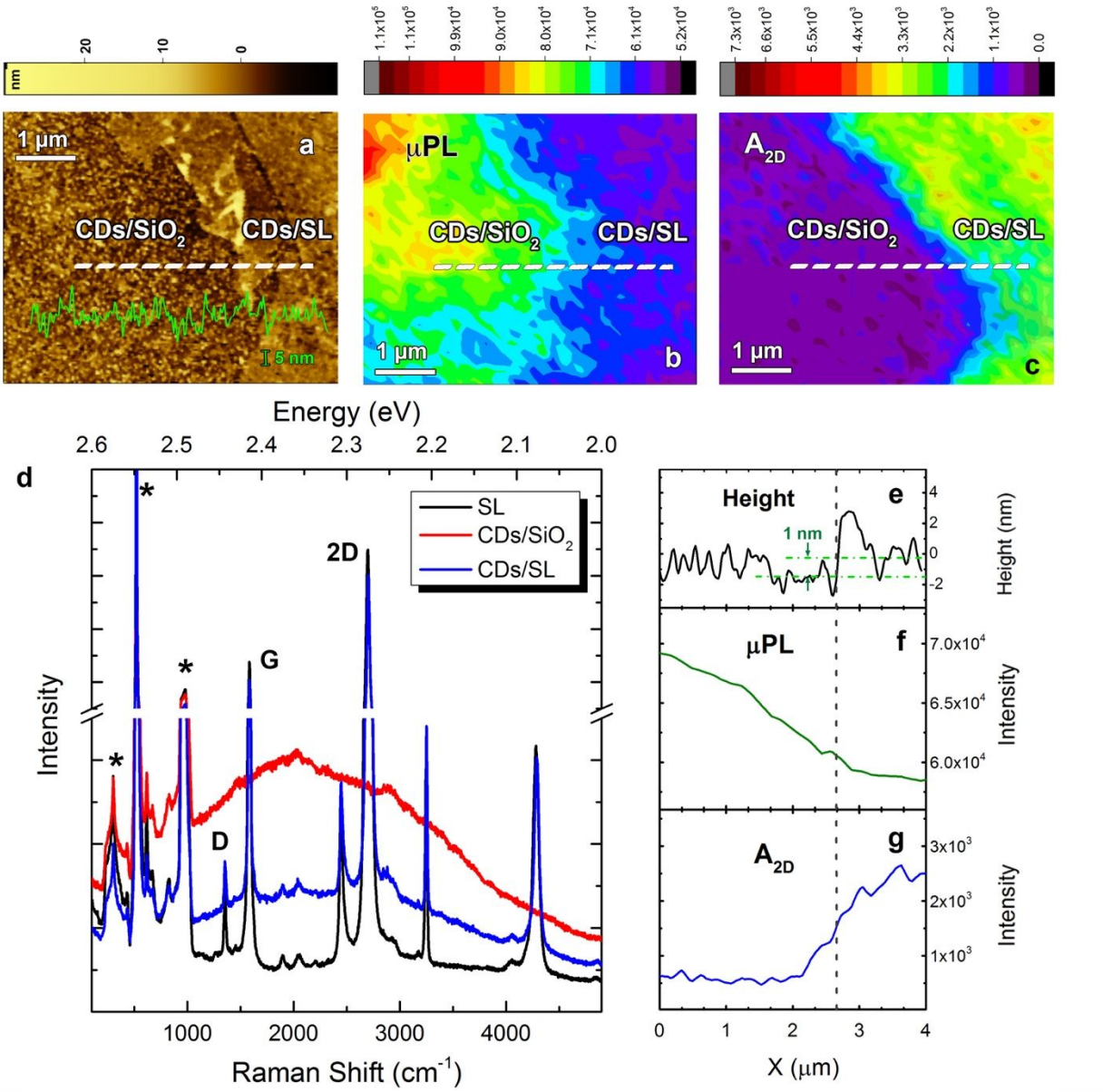

Figure 2. Co-localized AFM/Raman measurement of graphene on SiO_2/Si sample uniformly spread with CDs. (a) 7 µm x 6 µm AFM topography image showing the edge of the graphene sheet over the SiO_2/Si substrate. µPL (b) and A_{2D} Raman (c) maps of the same area as in (a). (d) Raman/µPL spectra of CDs deposited on SiO_2/Si substrate (red) and on graphene (blue), the Raman spectrum of naked graphene is reported for comparison (black). Stars on the graph indicate the Si Raman peaks. (e-g) Line profiles measured along the dashed lines in panels a-c. Please note that the height profile in Figure 2e is the same as the green profile in Figure 2a, but smoothed in order to highlight the graphene thickness.

BL graphene grown by CVD often consists of a mixture of perfectly oriented stacked layers (AB configuration, AB-BL) and misoriented stacked layers (twisted bilayers, t-BLs). Moreover, due to

polycrystalline nature of CVD graphene, each t-BL can be composed of domains with different twist angles.[21]

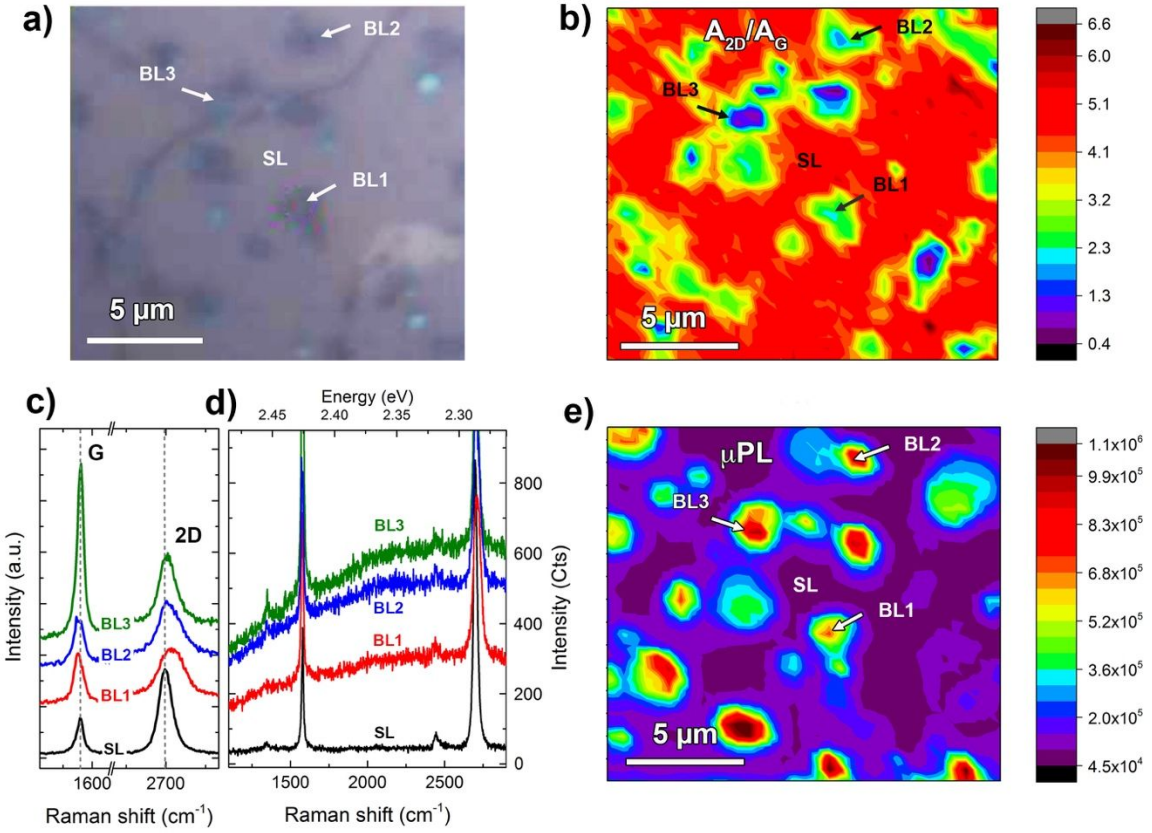

Figure 3. (a) Optical image of single/double CVD graphene coated with CDs. (b) A_{2D}/A_G Raman map correspondent to the same region shown in panel (a). (c) Raman spectra of BL and SL graphene highlighting the different G and 2D peak features. Spectra are offset for clarity. (d) Raman/μPL spectra of the same BLs displayed in panel (c) highlighting the higher photoluminescence as compared to SL graphene (black line). The measurements are taken in the points labeled in Figures 2b and 2e. (e) μPL map correspondent to the same region shown in panel (a).

Raman spectroscopy has proven to be a powerful technique for identifying the stacking order in multilayer graphene.[21,56] In t-BLs, Raman features show modifications that are related to the twist angle.[21,56] Those changes mainly concern position, width and integrated intensity of the 2D peak, while position and width of G peak are essentially angle independent.[56] Consequently, the A_{2D}/A_G

ratio will be also strongly affected by the twist angle. In particular, values of the A_{2D}/A_G ratio lower than the typical value of ~4.5 measured in SL graphene on SiO_2[61] are characteristic of the small angle range ($\theta \lesssim 11°$, for 473 nm laser wavelength), while higher values of the A_{2D}/A_G ratio compared to the SL graphene are observed in the large angle range ($\theta \gtrsim 15°$, for 473 nm laser wavelength).

In this framework a large area of the sample (about 250 μm^2), of which an optical image is shown in **Figure 3a**, was analyzed by Raman spectroscopy in order to assess the degree of heterogeneity in BL stacking order present in our sample. The changes in color observed in the A_{2D}/A_G Raman map of **Figure 3b** point out the presence of t-BLs with different twist angles as confirmed by the features of the *G* and *2D* Raman bands of different BLs (labeled in **Figure 3b** with BL1, BL2 and BL3), if compared with the SL case (**Figure 3c**). **Table 1** summarizes the results observed. *2D* peak in BL graphene undergoes a blue shift (up to 12 cm^{-1}) from the SL graphene *2D* position value (2702 cm^{-1}) while the *2D* full width half maximum (FWHM) can increases from 30 cm^{-1} (SL graphene) up to 55 cm^{-1} for BL1. These evidences, combined with the A_{2D}/A_G ratio, can give important information about the twist angle.[21,56] In particular BL1 and BL2 have a A_{2D}/A_G ratio of about 2.5, meaning $\theta \lesssim 11°$ (small angles - θ_S). [56] On the other side BL3 presents an even lower A_{2D}/A_G ratio (~ 1) because *G* peak intensity is higher (*G* peak area - A_G - is ~4.5 times higher than the SL graphene case).

Table 1 – Characteristic values of the Raman peaks of spectra showed in Figure 3c acquired in correspondence of the labels indicated in Figure 3a

	G Peak Position (cm^{-1})	G Peak FWHM (cm^{-1})	2D Peak Position (cm^{-1})	2D Peak FWHM (cm^{-1})	A_{2D}/A_G
CDs/SL	1582	14	2702	30	4.5
CDs/BL1	1579	19	2714	55	2.3
CDs/BL2	1580	19	2710	46	2.5
CDs/BL3	1583	13	2706	34	1.0

The G peak enhancement can be ascribed to the proximity of θ to the so-called critical angle θ_C, whose value depends on the laser excitation energy. However in this case θ does not yet fully matches θ_C (expected to be $\theta_C \cong 13°$ in our experimental conditions[56]), as the enhancement of A_G at the critical twist angle is nearly 30-fold compared to the one observable for a SL graphene. [56,62] The A_G amplification at θ_C happens because the excitation laser energy matches the energy difference between the conduction and the valence Van Hove singularity, giving rise to resonance effects.[56] Another clue of the fact that the BL3 twist angle is near θ_C is the modest *2D* shift (~2 cm^{-1}) from the SL graphene value, in agreement with other reports.[56] In other regions of the same sample, t-BL graphene with twist angle near θ_C were found, of which an optical image and representative Raman mapping are displayed in **Figure S4 a, b, d and e**. Looking at **Figure 3d** we notice the BLs Raman spectra have a notable PL band, centered at around 2.32 eV, which is due to the presence of CDs on top of the graphene substrate. As mentioned above, the emission of CDs is affected by the substrate they are deposited on.[17,45,60] In fact, for the spectra acquired on BL graphene the integrated μPL area (from 1120 cm^{-1} to 2980 cm^{-1}) is about 10 times more intense compared to the case of SL graphene (black line in **Figure 3d**). **Figure 3e** shows the μPL map associated to the spectra recorded within the area of **Figure 3a**. The emission is systematically

higher on top of BL graphene while it is quenched on SL graphene, as evident comparing μPL map (**Figure 3e**) with **Figure 3b**.

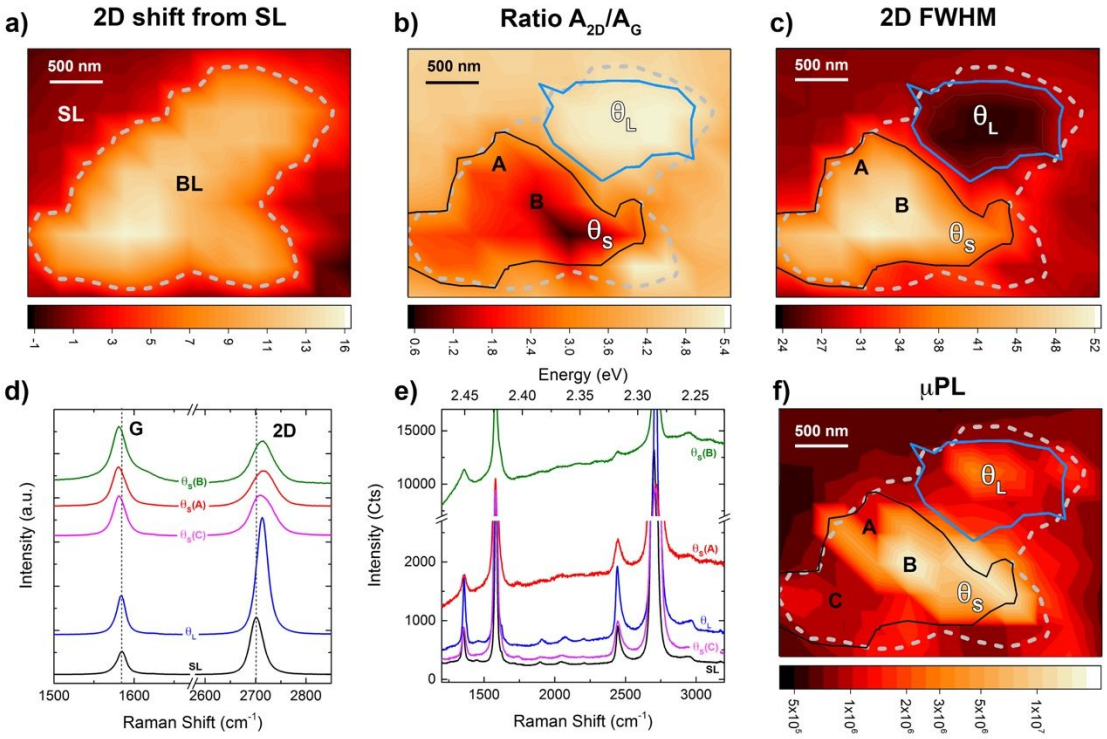

Figure 4. Spectral mapping of a BL graphene domain covered with CDs (red box in figure S.4a) showing (a) the 2D phonon shift (in cm^{-1}) with respect to case of SL, (b) A_{2D}/A_G ratio, (c) the 2D peak FWHM (in cm^{-1}). (d) Raman spectra of different zones inside the BL area and SL graphene highlighting the spectral features of the G and 2D peaks. Spectra are averaged over 4 close points and offset for clarity. (e) Raman/μPL spectra of the same zones displayed in panel (d) highlighting the higher photoluminescence as compared to SL graphene (black line). (f) μPL map over the analyzed region.

In order to have a close look to the correlation between the CDs emission and the BL graphene substrate, we analyzed with more detail and spatial resolution some individual BL areas. A leading example is the BL graphene enclosed in the red rectangle in **Figure S4a**. By simply looking at the *2D* peak shift compared to SL graphene (**Figure 4a)**, we identify a quite homogeneous BL graphene over a wider SL graphene area. However, the correspondent mapping of A_{2D}/A_G ratio as well as the *2D* FWHM, shown respectively in **Figure 4b** and **4c**, point out the presence of two

different main adjoining regions within the BL graphene which are clearly characterized by two different twist angles θ. Notably the region enclosed in the black contour is characterized by a small A_{2D}/A_G ratio (between 1 and 2.4) and by a high FWHM ($\sim$55 cm^{-1}). These quantities allow us to assume the BL twist angle is in the range of θ_S.[56] Moreover, such different values of A_{2D}/A_G together with the fact that the FWHM of *2D* has a quite large distribution (green bars in **Figure S3**), may suggest the presence of further adjacent domains, within the black contoured zone, with different twist angles. However, by comparing the spectra acquired in correspondence of $\theta_S(A)$ and $\theta_S(B)$ in **Figure 4b**, red and green line in **Figure 4d** respectively, we are not able to highlight any significant difference in the spectral features of the *2D* peak. In any case we can claim that the black bounded area has $\theta_S \lesssim 11°$ even if our analysis approach is not enough detailed to have a more precise identification of the twist angles. On the other side, the contiguous area enclosed in the blue line in **Figure 4b** and **Figure 4c** is characterized by a A_{2D}/A_G ratio of 5.2 (higher than the SL graphene A_{2D}/A_G ratio) and by a narrow 2D peak featuring a FWHM of 27 cm^{-1}, even lower than the SL graphene case (red bars in **Figure S3**). These spectral properties, together with the *2D* peak shift of about 10 cm^{-1}, suggest that the twist angle is quite high (indicated henceforth as θ_L), which in general, in our experimental conditions is $\theta_L \gtrsim 15°$.[56] In this case the coupling parameter between the two overlapping layers is weaker than the one characterizing BL(θ_S) and therefore BL(θ_L) behaves nearly like two SL graphene sheets.[33] A typical Raman spectrum of the BL(θ_L) graphene is represented by the blue line in **Figure 4d**.

It is noteworthy that the adjoining BL(θ_S) and BL(θ_L) regions show also a different response while interacting with the CDs. Typical micro Raman/PL spectra for BL(θ_S) and BL(θ_L) are represented in **Figure 4e**. As highlighted in **Figure 4f** CDs μPL signal is considerably large and almost confined in the BL(θ_S) area (black contoured region in **Figure 4f**), while it is quite small (2.5 times

weaker than BL(θ_S)) in the BL(θ_L) area (blue contoured region in **Figure 4f**) even if it is still 2.5 times higher than the fluorescence background of SL graphene (black line in **Figure 4e**). A large μPL signal, similar to that relative to the BL(θ_S) area, was also measured for CDs deposited on t-BL with twist angle near θ_C, as shown in **Figure S4c**.

Finally, we also want to draw the attention to the region labeled as θ_S(C) in **Figure 4f.** This region is evidently characterized by a small θ but the CDs μPL emission in this case is quite low and in contrast with what we observed for θ_S(A) (see red and pink line in **Figure 4e**). However comparing the 2D spectral properties of θ_S(A) and θ_S(C) (**Figure S5**), we can notice that in the latter case *2D* peak is slightly asymmetric and can be described with four bands contributions suggesting the proximity to zero of the twist angle, *i.e.* the AB-BL.[57]

Therefore the strong interaction between the two overlapping graphene layers[33] can actively influence the μPL emission of CDs interacting with BL graphene as summarized in **Figure S6**.

3.2 CDs/BL graphene interaction

The structural and emission properties of CDs deposited on SL graphene were previously investigated.[17,45] It has been shown that the PL quenching of CDs deposited on SL graphene can be explained invoking the interaction between the surface states of CDs, responsible of the emission process,[48,63] and the band structure of graphene.[45] Briefly, thanks to the close contact between the excited surface states of CDs and the SL graphene conduction band, photoelectrons, generated by the absorption process at energies greater than 2 eV, can be transferred from CDs to SL graphene.[60]

The electronic band structure of t-BL is quite different from that of SL graphene and of AB-BL. Single layer graphene is a semimetal with a linear band structure (at the K point in the Brillouin zone (Dirac cone)).[64] In pristine SL graphene, the Fermi energy (E_F) is at K=0 and its position can be tuned by chemical doping[65,66] or by gating.[12] In AB-BL graphene the band structure changes to become parabolic and a gap can open by applying vertical electric fields[67] or by doping.[68] When a stacking defect is present in a BL, such as a twist angle between the layers, the electronic band structure changes further. The band structure of t-BL graphene consists of two nearby Dirac cones, one from top layer and the other from bottom one, separated from each other by a distance that increases with the twist angle. Experimental[28,39] and theoretical[20] works demonstrated that the linear band structure is preserved at the Dirac point, as in a SL graphene, but at small angle (below θ_C) the Fermi velocity reduces with respect to SL graphene;[69] moreover, it has been showed that an external electric field does not open a gap in the band structure.[20]

In t-BL graphene, the electronic interlayer coupling rapidly decreases as the twist angle increases[38] and at large twist angle (above θ_C) the electronic properties become more similar to those of a SL graphene.[39]

The interpretative model of the interaction between CDs and t-BL graphene is explained below. The interaction between CDs and t-BL graphene is strongly influenced by the degree of interlayer coupling. Two charge transfer mechanisms, radiative and non-radiative, can occur at the same time and the prevalence of one over the other is linked to the interlayer coupling and then to Fermi velocity renormalization.[39]

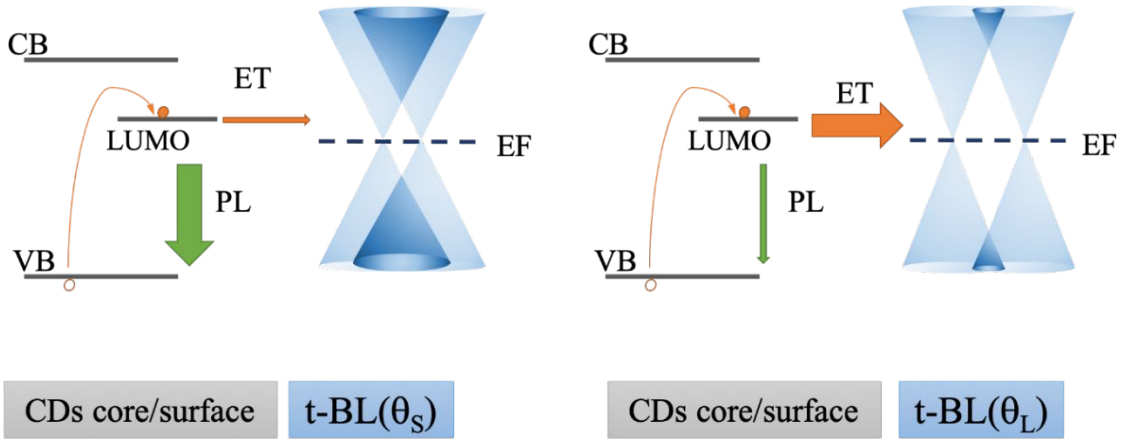

Figure 5 Pictorial representation of the band structures of BL graphene with small twist angle (left) and large twist angle (right) together with the surface lowest unoccupied molecular orbital (LUMO) and band structure of CDs. The Fermi level (EF) of graphene is highlighted by dashed line and the electron transfer process (ET) by orange arrows. The PL process is evidenced by green arrows. The effectiveness of each process is marked by the size of the arrows. Photoexcitation induces an electron extraction from valence band (VB) of CDs core to LUMO CDs surface state and successively an ET process to graphene.

When CDs are in close contact with t-BL graphene (**Figure 5**), the electrons photoexcited in the surface states of the CDs can be transferred either to the conduction band of t-BL graphene (non-radiative process) or to the CDs core states giving rise to the typical process of photoluminescence of CDs. The non-radiative electron transfer (ET) prevails when the CDs are in contact with large twist angle (θ_L) graphene bilayer **(Figure 5, right)**. In this case, the interlayer coupling is very weak and Fermi velocity does not undergo significant variations with respect to its SL graphene value, so the t-BL behaves almost like a SL graphene. At small twist angles (θ_S), the coupling between the planes increases; thus, we hypothesize that the lower Fermi velocity of the electrons causes a inhibition of the process of non-radiative charge transfer from the CDs to the t-BL graphene thus favoring the PL process (**Figure 5, left**). According to this model, the different values of the PL emission of the CDs observed in the BL (θ_S) region enclosed in the black contour in **Figure 4f** are ascribed to different values of θ_S. In particular, at very small values of θ_S the

radiative electron transfer prevails due to the very low Fermi velocity and thus a significant increment in the CDs PL emission occurs. In BL (θ_L) graphene and AB-BL graphene (θ=0°) there is no reduction of the Fermi velocity[36,70] and therefore the non-radiative electron transfer (ET) is not inhibited, which translates in a quenching of the CDs PL (**Figure 4f**).

To summarize, the CDs photoemission efficiency is still significant when they are in close contact with BL (θ_S) graphene. On the contrary when they are interacting with SL graphene, AB-BL or BL (θ_L) graphene, a considerable μPL quenching is observed (**Figure S6**).

4. CONCLUSION

In summary, we performed a systematic micro Raman/PL characterization on a composite material in solid phase obtained by drop casting CDs on single and bilayer CVD graphene supported on a SiO_2/Si substrate. Raman analysis revealed the occurrence of different twisted BL graphene each composed of domains with different twist angle. A detailed micro-PL study revealed that the emission efficiency of the CDs deposited on t-BL graphene is strongly dependent on the twist angle. The interaction between CDs and t-BL/SiO_2 substrate was explained by considering the competition between two electron transfer mechanisms, a radiative and a non-radiative. The degree of interlayer coupling, and therefore the renormalization of the Fermi velocity, is the key factor that determines the prevalence of one charge transfer mechanism over the other. These results encourage further investigations on such CDs/BL graphene composites for applications in optoelectronic and light-harvesting nano-devices.

ASSOCIATED CONTENT

Supporting Information.

The following files are available free of charge.

Additional optical images, AFM images, Raman/PL maps, peak fitting of Raman spectra

AUTHOR INFORMATION

Corresponding Author

* E-mail: gfaggio@unirc.it (Giuliana Faggio)

Author Contributions

The manuscript was written through contributions of all authors. All authors have given approval to the final version of the manuscript.

Funding Sources

This publication is co-financed with the support of the European Commission, the European Social Fund and the Calabria Region (CUP: C31J19000010002). This research was also supported by the MIUR PRIN 2017 - CANDL2 project and by the AIM1839112-1 project funded within the Attraction and International Mobility (AIM) program (CUP: C35E19000020001).

REFERENCES

(1) Zeng, X.; Wang, Z.; Meng, N.; McCarthy, D. T.; Deletic, A.; Pan, J. hong; Zhang, X. Highly Dispersed TiO2 Nanocrystals and Carbon Dots on Reduced Graphene Oxide: Ternary Nanocomposites for Accelerated Photocatalytic Water Disinfection. *Appl. Catal. B Environ.* **2017**, *202*, 33–41. https://doi.org/10.1016/j.apcatb.2016.09.014.

(2) Raja, A.; Montoya-Castillo, A.; Zultak, J.; Zhang, X. X.; Ye, Z.; Roquelet, C.; Chenet, D.

A.; Van Der Zande, A. M.; Huang, P.; Jockusch, S.; et al. Energy Transfer from Quantum Dots to Graphene and MoS2: The Role of Absorption and Screening in Two-Dimensional Materials. *Nano Lett.* **2016**, *16*, 2328–2333. https://doi.org/10.1021/acs.nanolett.5b05012.

(3) Li, X.; Rui, M.; Song, J.; Shen, Z.; Zeng, H. Carbon and Graphene Quantum Dots for Optoelectronic and Energy Devices: A Review. *Adv. Funct. Mater.* **2015**, *25* (31), 4929–4947. https://doi.org/10.1002/adfm.201501250.

(4) Xu, X.; Ray, R.; Gu, Y.; Ploehn, H. J.; Gearheart, L.; Raker, K.; Scrivens, W. A. Electrophoretic Analysis and Purification of Fluorescent Single-Walled Carbon Nanotube Fragments. *J. Am. Chem. Soc.* **2004**, *126* (40), 12736–12737. https://doi.org/10.1021/ja040082h.

(5) Sciortino, A.; Cayuela, A.; Soriano, M. L.; Gelardi, F. M.; Cannas, M.; Valcárcel, M.; Messina, F. Different Natures of Surface Electronic Transitions of Carbon Nanoparticles. *Phys. Chem. Chem. Phys.* **2017**, *19*, 22670–22677. https://doi.org/10.1039/c7cp04548d.

(6) Liu, J.; Liu, Y.; Liu, N.; Han, Y.; Zhang, X.; Huang, H.; Lifshitz, Y.; Lee, S. T.; Zhong, J.; Kang, Z. Metal-Free Efficient Photocatalyst for Stable Visible Water Splitting via a Two-Electron Pathway. *Science (80-.).* **2015**, *347* (6225), 970–974. https://doi.org/10.1126/science.aaa3145.

(7) Kwon, W.; Lee, G.; Do, S.; Joo, T.; Rhee, S. W. Size-Controlled Soft-Template Synthesis of Carbon Nanodots toward Versatile Photoactive Materials. *Small* **2014**, *10* (3), 506–513. https://doi.org/10.1002/smll.201301770.

(8) Sun, M.; Qu, S.; Hao, Z.; Ji, W.; Jing, P.; Zhang, H.; Zhang, L.; Zhao, J.; Shen, D. Towards Efficient Solid-State Photoluminescence Based on Carbon-Nanodots and Starch Composites. *Nanoscale* **2014**, *6*, 13076–13081. https://doi.org/10.1039/c4nr04034a.

(9) Mirtchev, P.; Henderson, E. J.; Soheilnia, N.; Yip, C. M.; Ozin, G. A. Solution Phase Synthesis of Carbon Quantum Dots as Sensitizers for Nanocrystalline TiO2 Solar Cells. *J. Mater. Chem.* **2012**, *22*, 1265–1269. https://doi.org/10.1039/c1jm14112k.

(10) Yu, X.; Liu, J.; Yu, Y.; Zuo, S.; Li, B. Preparation and Visible Light Photocatalytic Activity of Carbon Quantum Dots/TiO2 Nanosheet Composites. *Carbon N. Y.* **2014**, *68*, 718–724. https://doi.org/10.1016/j.carbon.2013.11.053.

(11) Bian, H.; Wang, Q.; Yang, S.; Yan, C.; Wang, H.; Liang, L.; Jin, Z.; Wang, G.; Liu, S. Nitrogen-Doped Graphene Quantum Dots for 80% Photoluminescence Quantum Yield for Inorganic γ-CsPbI3 Perovskite Solar Cells with Efficiency beyond 16%. *J. Mater. Chem. A* **2019**, *7* (10), 5740–5747. https://doi.org/10.1039/c8ta12519h.

(12) Novoselov, K. S.; Geim, A. K.; Morozov, S. V; Jiang, D.; Zhang, Y.; Dubonos, S. V; Grigorieva, I. V; Firsov, A. A. Electric Field Effect in Atomically Thin Carbon Films. *Science* **2004**, *306* (5696), 666–669. https://doi.org/10.1126/science.1102896.

(13) Bae, S.; Kim, H.; Lee, Y.; Xu, X.; Park, J.-S.; Zheng, Y.; Balakrishnan, J.; Lei, T.; Kim, H. R.; Song, Y. Il; et al. Roll-to-Roll Production of 30-Inch Graphene Films for Transparent Electrodes. *Nat. Nanotechnol.* **2010**, *5*, 574–578. https://doi.org/10.1038/nnano.2010.132.

(14) Bonaccorso, F.; Sun, Z.; Hasan, T.; Ferrari, A. C. Graphene Photonics and Optoelectronics. *Nat. Photonics* **2010**, *4*, 611–622. https://doi.org/10.1038/nphoton.2010.186.

(15) Belviso, S.; Capasso, A.; Santoro, E.; Najafi, L.; Lelj, F.; Superchi, S.; Casarini, D.; Villani, C.; Spirito, D.; Bellani, S.; et al. Thioethyl-Porphyrazine/Nanocarbon Hybrids for Photoinduced Electron Transfer. *Adv. Funct. Mater.* **2018**, *28* (21), 1705418. https://doi.org/10.1002/adfm.201705418.

(16) Faggio, G.; Capasso, A.; Messina, G.; Santangelo, S.; Dikonimos, T.; Gagliardi, S.; Giorgi,

R.; Morandi, V.; Ortolani, L.; Lisi, N. High-Temperature Growth of Graphene Films on Copper Foils by Ethanol Chemical Vapor Deposition. *J. Phys. Chem. C* **2013**, *117* (41), 21569–21576. https://doi.org/10.1021/jp407013y.

(17) Faggio, G.; Gnisci, A.; Messina, G.; Lisi, N.; Capasso, A.; Lee, G. H.; Armano, A.; Sciortino, A.; Messina, F.; Cannas, M.; et al. Carbon Dots Dispersed on Graphene/SiO2/Si: A Morphological Study. *Phys. Status Solidi Appl. Mater. Sci.* **2019**, *216* (3), 1800559. https://doi.org/10.1002/pssa.201800559.

(18) Berger, C.; Song, Z.; Li, X.; Wu, X.; Brown, N.; Naud, C.; Mayou, D.; Li, T.; Hass, J.; Marchenkov, A. N.; et al. Electronic Confinement and Coherence in Patterned Epitaxial Graphene. *Science* **2006**, *312*, 1191–1196. https://doi.org/10.1126/science.1125925.

(19) Li, X.; Cai, W.; An, J.; Kim, S.; Nah, J.; Yang, D.; Piner, R.; Velamakanni, A.; Jung, I.; Tutuc, E.; et al. Large-Area Synthesis of High-Quality and Uniform Graphene Films on Copper Foils. *Science* **2009**, *324* (5932), 1312–1314. https://doi.org/10.1126/science.1171245.

(20) Lopes Dos Santos, J. M. B.; Peres, N. M. R.; Castro Neto, A. H. Graphene Bilayer with a Twist: Electronic Structure. *Phys. Rev. Lett.* **2007**, *99* (25), 19–22. https://doi.org/10.1103/PhysRevLett.99.256802.

(21) Havener, R. W.; Zhuang, H.; Brown, L.; Hennig, R. G.; Park, J. Angle-Resolved Raman Imaging of Interlayer Rotations and Interactions in Twisted Bilayer Graphene. *Nano Lett.* **2012**, *12* (6), 3162–3167. https://doi.org/10.1021/nl301137k.

(22) Bistritzer, R.; MacDonald, A. H. Moiré Bands in Twisted Double-Layer Graphene. *Proc. Natl. Acad. Sci. U. S. A.* **2011**, *108* (30), 12233–12237. https://doi.org/10.1073/pnas.1108174108.

(23) Lui, C. H.; Li, Z.; Mak, K. F.; Cappelluti, E.; Heinz, T. F. Observation of an Electrically Tunable Band Gap in Trilayer Graphene. *Nat. Phys.* **2011**, *7* (12), 944–947. https://doi.org/10.1038/NPHYS2102.

(24) Brown, L.; Hovden, R.; Huang, P.; Wojcik, M.; Muller, D. A.; Park, J. Twinning and Twisting of Tri- and Bilayer Graphene. *Nano Lett.* **2012**, *12* (3), 1609–1615. https://doi.org/10.1021/nl204547v.

(25) Reina, A.; Jia, X.; Ho, J.; Nezich, D.; Son, H.; Bulovic, V.; Dresselhaus, M. S.; Kong, J. Large Area, Few-Layer Graphene Films on Arbitrary Substrates by Chemical Vapor Deposition. *Nano Lett.* **2009**, *9* (1), 30–35. https://doi.org/10.1021/nl801827v.

(26) Liu, J. B.; Li, P. J.; Chen, Y. F.; Wang, Z. G.; Qi, F.; He, J. R.; Zheng, B. J.; Zhou, J. H.; Zhang, W. L.; Gu, L.; et al. Observation of Tunable Electrical Bandgap in Large-Area Twisted Bilayer Graphene Synthesized by Chemical Vapor Deposition. *Sci. Rep.* **2015**, *5*, 15285. https://doi.org/10.1038/srep15285.

(27) Ramnani, P.; Neupane, M. R.; Ge, S.; Balandin, A. A.; Lake, R. K.; Mulchandani, A. Raman Spectra of Twisted CVD Bilayer Graphene. *Carbon N. Y.* **2017**, *123*, 302–306. https://doi.org/10.1016/j.carbon.2017.07.064.

(28) Li, G.; Luican, A.; Lopes Dos Santos, J. M. B.; Castro Neto, A. H.; Reina, A.; Kong, J.; Andrei, E. Y. Observation of Van Hove Singularities in Twisted Graphene Layers. *Nat. Phys.* **2010**, *6* (2), 109–113. https://doi.org/10.1038/nphys1463.

(29) Charlier, J. C.; Michenaud, J. P.; Gonze, X. First-Principles Study of the Electronic Properties of Simple Hexagonal Graphite. *Phys. Rev. B* **1992**, *46* (8), 4531–4539. https://doi.org/10.1103/PhysRevB.46.4531.

(30) Liu, Z.; Suenaga, K.; Harris, P. J. F.; Iijima, S. Open and Closed Edges of Graphene Layers.

Phys. Rev. Lett. **2009**, *102* (1), 1–4. https://doi.org/10.1103/PhysRevLett.102.015501.

(31) Chen, Y. C.; Lin, W. H.; Tseng, W. S.; Chen, C. C.; Rossman, G. R.; Chen, C. D.; Wu, Y. S.; Yeh, N. C. Direct Growth of Mm-Size Twisted Bilayer Graphene by Plasma-Enhanced Chemical Vapor Deposition. *Carbon N. Y.* **2020**, *156*, 212–224. https://doi.org/10.1016/j.carbon.2019.09.052.

(32) He, R.; Chung, T. F.; Delaney, C.; Keiser, C.; Jauregui, L. A.; Shand, P. M.; Chancey, C. C.; Wang, Y.; Bao, J.; Chen, Y. P. Observation of Low Energy Raman Modes in Twisted Bilayer Graphene. *Nano Lett.* **2013**, *13* (8), 3594–3601. https://doi.org/10.1021/nl4013387.

(33) Suárez Morell, E.; Vargas, P.; Chico, L.; Brey, L. Charge Redistribution and Interlayer Coupling in Twisted Bilayer Graphene under Electric Fields. *Phys. Rev. B - Condens. Matter Mater. Phys.* **2011**, *84* (19), 195421. https://doi.org/10.1103/PhysRevB.84.195421.

(34) Wang, Y.; Ni, Z.; Liu, L.; Liu, Y.; Cong, C.; Yu, T.; Wang, X.; Shen, D.; Shen, Z. Stacking-Dependent Optical Conductivity of Bilayer Graphene. *ACS Nano* **2010**, *4* (7), 4074–4080. https://doi.org/10.1021/nn1004974.

(35) Das Sarma, S.; Adam, S.; Hwang, E. H.; Rossi, E. Electronic Transport in Two-Dimensional Graphene. *Rev. Mod. Phys.* **2011**, *83* (2), 407–470. https://doi.org/10.1103/RevModPhys.83.407.

(36) Rozhkov, A. V.; Sboychakov, A. O.; Rakhmanov, A. L.; Nori, F. Electronic Properties of Graphene-Based Bilayer Systems. *Phys. Rep.* **2016**, *648*, 1–104. https://doi.org/10.1016/j.physrep.2016.07.003.

(37) Lu, C. C.; Lin, Y. C.; Liu, Z.; Yeh, C. H.; Suenaga, K.; Chiu, P. W. Twisting Bilayer Graphene Superlattices. *ACS Nano* **2013**, *7* (3), 2587–2594. https://doi.org/10.1021/nn3059828.

(38) Malard, L. M.; Pimenta, M. A.; Dresselhaus, G.; Dresselhaus, M. S. Raman Spectroscopy in Graphene. *Physics Reports*. 2009, pp 51–87. https://doi.org/10.1016/j.physrep.2009.02.003.

(39) Luican, A.; Li, G.; Reina, A.; Kong, J.; Nair, R. R.; Novoselov, K. S.; Geim, A. K.; Andrei, E. Y. Single-Layer Behavior and Its Breakdown in Twisted Graphene Layers. *Phys. Rev. Lett.* **2011**, *106* (12), 1–4. https://doi.org/10.1103/PhysRevLett.106.126802.

(40) Fang, W.; Hsu, A. L.; Song, Y.; Kong, J. A Review of Large-Area Bilayer Graphene Synthesis by Chemical Vapor Deposition. *Nanoscale* **2015**, *7* (48), 20335–20351. https://doi.org/10.1039/c5nr04756k.

(41) Wang, J.; Mu, X.; Wang, L.; Sun, M. Properties and Applications of New Superlattice: Twisted Bilayer Graphene. *Mater. Today Phys.* **2019**, *9*. https://doi.org/10.1016/j.mtphys.2019.100099.

(42) Wang, Y.; Myers, M.; Staser, J. A. Electrochemical UV Sensor Using Carbon Quantum Dot/Graphene Semiconductor. *J. Electrochem. Soc.* **2018**, *165* (4), H3001–H3007. https://doi.org/10.1149/2.0011804jes.

(43) Chen, X.; Yang, C.; Sun, H.; Ning, S.; Zhou, H.; Zhang, H.; Wang, S.; Feng, G.; Zhou, S. Enhanced Photoresponsivity in Carbon Quantum Dots-Coupled Graphene/Silicon Schottky-Junction Photodetector. *Laser Phys. Lett.* **2019**, *16* (7), 1–7. https://doi.org/10.1088/1612-202X/ab2040.

(44) Wang, Q.; Jin, Z.; Chen, D.; Bai, D.; Bian, H.; Sun, J.; Zhu, G.; Wang, G.; Liu, S. (Frank). M-Graphene Crosslinked CsPbI3 Quantum Dots for High Efficiency Solar Cells with Much Improved Stability. *Adv. Energy Mater.* **2018**, *8* (22), 1–8. https://doi.org/10.1002/aenm.201800007.

(45) Armano, A.; Buscarino, G.; Messina, F.; Sciortino, A.; Cannas, M.; Gelardi, F. M.; Giannazzo, F.; Schilirò, E.; Agnello, S. Photoinduced Charge Transfer from Carbon Dots to Graphene in Solid Composite. *Thin Solid Films* **2019**, *669* (August 2018), 620–624. https://doi.org/10.1016/j.tsf.2018.11.049.

(46) Li, X.; Zhu, Y.; Cai, W.; Borysiak, M.; Han, B.; Chen, D.; Piner, R. D.; Colomba, L.; Ruoff, R. S. Transfer of Large-Area Graphene Films for High-Performance Transparent Conductive Electrodes. *Nano Lett.* **2009**, *9* (12), 4359–4363. https://doi.org/10.1021/nl902623y.

(47) Liang, X.; Sperling, B. A.; Calizo, I.; Cheng, G.; Hacker, C. A.; Zhang, Q.; Obeng, Y.; Yan, K.; Peng, H.; Li, Q.; et al. Toward Clean and Crackless Transfer of Graphene. *ACS Nano* **2011**, *5* (11), 9144–9153. https://doi.org/10.1021/nn203377t.

(48) Messina, F.; Sciortino, L.; Popescu, R.; Venezia, A. M.; Sciortino, A.; Buscarino, G.; Agnello, S.; Schneider, R.; Gerthsen, D.; Cannas, M.; et al. Fluorescent Nitrogen-Rich Carbon Nanodots with an Unexpected β-C3N4 Nanocrystalline Structure. *J. Mater. Chem. C* **2016**, *4*, 2598. https://doi.org/10.1039/c5tc04096e.

(49) Sciortino, A.; Mauro, N.; Buscarino, G.; Sciortino, L.; Popescu, R.; Schneider, R.; Giammona, G.; Gerthsen, D.; Cannas, M.; Messina, F. β-C3N4 Nanocrystals: Carbon Dots with Extraordinary Morphological, Structural, and Optical Homogeneity. *Chem. Mater.* **2018**, *30* (5), 1695–1700. https://doi.org/10.1021/acs.chemmater.7b05178.

(50) *Noncontact Atomic Force Microscopy*; Morita, S., Wiesendanger, R., Meyer, E., Eds.; Springer-Verlag Berlin Heidelberg, 2002. https://doi.org/10.1007/978-3-662-02882-7.

(51) Blake, P.; Hill, E. W.; Castro Neto, A. H.; Novoselov, K. S.; Jiang, D.; Yang, R.; Booth, T. J.; Geim, A. K. Making Graphene Visible. *Appl. Phys. Lett.* **2007**, *91* (6).

https://doi.org/10.1063/1.2768624.

(52) Gupta, A.; Chen, G.; Joshi, P.; Tadigadapa, S.; Eklund, P. C. Raman Scattering from High-Frequency Phonons in Supported n-Graphene Layer Films. *Nano Lett.* **2006**, *6* (12), 2667–2673. https://doi.org/10.1021/nl061420a.

(53) Nemes-Incze, P.; Osváth, Z.; Kamarás, K.; Biró, L. P. Anomalies in Thickness Measurements of Graphene and Few Layer Graphite Crystals by Tapping Mode Atomic Force Microscopy. *Carbon N. Y.* **2008**, *46* (11), 1435–1442. https://doi.org/10.1016/j.carbon.2008.06.022.

(54) Yan, K.; Peng, H.; Zhou, Y.; Li, H.; Liu, Z. Formation of Bilayer Bernal Graphene: Layer-by-Layer Epitaxy via Chemical Vapor Deposition. *Nano Lett.* **2011**, *11* (3), 1106–1110. https://doi.org/10.1021/nl104000b.

(55) Girifalco, L. A.; Lad, R. A. Energy of Cohesion, Compressibility, and the Potential Energy Functions of the Graphite System. *J. Chem. Phys.* **1956**, *25*, 693. https://doi.org/10.1063/1.1743030.

(56) Kim, K.; Coh, S.; Tan, L. Z.; Regan, W.; Yuk, J. M.; Chatterjee, E.; Crommie, M. F.; Cohen, M. L.; Louie, S. G.; Zettl, A. Raman Spectroscopy Study of Rotated Double-Layer Graphene: Misorientation-Angle Dependence of Electronic Structure. *Phys. Rev. Lett.* **2012**, *108* (24), 1–6. https://doi.org/10.1103/PhysRevLett.108.246103.

(57) Ferrari, A. C.; Meyer, J. C.; Scardaci, V.; Casiraghi, C.; Lazzeri, M.; Mauri, F.; Piscanec, S.; Jiang, D.; Novoselov, K. S.; Roth, S.; et al. Raman Spectrum of Graphene and Graphene Layers. *Phys. Rev. Lett.* **2006**, *97* (18), 187401. https://doi.org/10.1103/PhysRevLett.97.187401.

(58) Eckmann, A.; Felten, A.; Mishchenko, A.; Britnell, L.; Krupke, R.; Novoselov, K. S.;

Casiraghi, C. Probing the Nature of Defects in Graphene by Raman Spectroscopy. *Nano Lett.* **2012**, *12* (8), 3925–3930. https://doi.org/10.1021/nl300901a.

(59) Uchinokura, K.; Sekine, T.; Matsuura, E. Raman Scattering by Silicon. *Solid State Commun.* **1972**, *11* (1), 47–49. https://doi.org/10.1016/0038-1098(72)91127-1.

(60) Armano, A.; Buscarino, G.; Messina, F.; Sciortino, A.; Cannas, M.; Gelardi, F. M.; Giannazzo, F.; Schilirò, E.; Agnello, S. Dynamic Modification of Fermi Energy in Single-Layer Graphene by Photoinduced Electron Transfer from Carbon Dots. *Nanomaterials* **2020**, *10* (3), 528. https://doi.org/10.3390/nano10030528.

(61) Wang, Q. H.; Jin, Z.; Kim, K. K.; Hilmer, A. J.; Paulus, G. L. C.; Shih, C. J.; Ham, M. H.; Sanchez-Yamagishi, J. D.; Watanabe, K.; Taniguchi, T.; et al. Understanding and Controlling the Substrate Effect on Graphene Electron-Transfer Chemistry via Reactivity Imprint Lithography. *Nat. Chem.* **2012**, *4*, 724 –732. https://doi.org/10.1038/nchem.1421.

(62) Huang, S.; Yankowitz, M.; Chattrakun, K.; Sandhu, A.; Leroy, B. J. Evolution of the Electronic Band Structure of Twisted Bilayer Graphene upon Doping. *Sci. Rep.* **2017**, *7*, 7611. https://doi.org/10.1038/s41598-017-07580-3.

(63) Sciortino, A.; Marino, E.; Dam, B. Van; Schall, P.; Cannas, M.; Messina, F. Solvatochromism Unravels the Emission Mechanism of Carbon Nanodots. *J. Phys. Chem. Lett.* **2016**, *7* (17), 3419–3423. https://doi.org/10.1021/acs.jpclett.6b01590.

(64) Castro Neto, A. H. .; Peres, N. M. R. .; Novoselov, K. S. .; Geim, A. K. .; Guinea, F. The Electronic Properties of Graphene. *Rev. Mod. Phys.* **2009**, *81* (1), 109–162. https://doi.org/10.1103/RevModPhys.81.109.

(65) Hwang, E. H.; Adam, S.; Das Sarma, S. Transport in Chemically Doped Graphene in the Presence of Adsorbed Molecules. *Phys. Rev. B - Condens. Matter Mater. Phys.* **2007**, *76*,

195421–195426. https://doi.org/10.1103/PhysRevB.76.195421.

(66) Dong, X.; Fu, D.; Fang, W.; Shi, Y.; Chen, P.; Li, L. J. Doping Single-Layer Graphene with Aromatic Molecules. *Small* **2009**, *5* (12), 1422–1426. https://doi.org/10.1002/smll.200801711.

(67) Castro, E. V.; Novoselov, K. S.; Morozov, S. V.; Peres, N. M. R.; Dos Santos, J. M. B. L.; Nilsson, J.; Guinea, F.; Geim, A. K.; Neto, A. H. C. Biased Bilayer Graphene: Semiconductor with a Gap Tunable by the Electric Field Effect. *Phys. Rev. Lett.* **2007**, *99* (21), 216802–216805. https://doi.org/10.1103/PhysRevLett.99.216802.

(68) Ohta, T.; Bostwick, A.; Seyller, T.; Horn, K.; Rotenberg, E. Controlling the Electronic Structure of Bilayer Graphene. *Science (80-.).* **2006**, *313*, 951–954. https://doi.org/10.1126/science.1130681.

(69) Shallcross, S.; Sharma, S.; Kandelaki, E.; Pankratov, O. A. Electronic Structure of Turbostratic Graphene. *Phys. Rev. B - Condens. Matter Mater. Phys.* **2010**, *81* (1), 1–15. https://doi.org/10.1103/PhysRevB.81.165105.

(70) Berciaud, S.; Potemski, M.; Faugeras, C. Probing Electronic Excitations in Mono- to Pentalayer Graphene by Micro Magneto-Raman Spectroscopy. *Nano Lett.* **2014**, *14* (8), 4548–4553. https://doi.org/10.1021/nl501578m.